Aluminosilicate weak colloidal gels: from the early age to the precipitation of zeolite

Electronic Supplementary Information (ESI†)

Donatien Gomes Rodrigues[a], Bavand Keshavarz[b], Nicolas Courtois[c], Jan Ilavski[d], Gareth H. McKinley[b] and Arnaud Poulesquen[c*]

[a] *CEA, DES, ISEC, DMRC, Univ Montpellier, F-30207 Bagnols-sur-Cèze, France*
[b] *Hatsopoulos Microfluids Laboratory, Department of Mechanical Engineering, Massachusetts Institute of Technology, Cambridge, Massachusetts 02139, USA*
[c] *CEA, DES, ISEC, DPME, Univ Montpellier, F-30207 Bagnols-sur-Cèze, France*
[d] *Advanced Photon Source, Argonne National Laboratory, Lemont, Illinois 60439, USA*

[*] *Corresponding author:*
arnaud.poulesquen@cea.fr

1 Experimental set-up for rheological measurements

Figures S1 and S2 present the method of preparation of the gel and the associated rheological protocol, that allows monitoring the viscoelastic modulus in the linear region during the gelation.

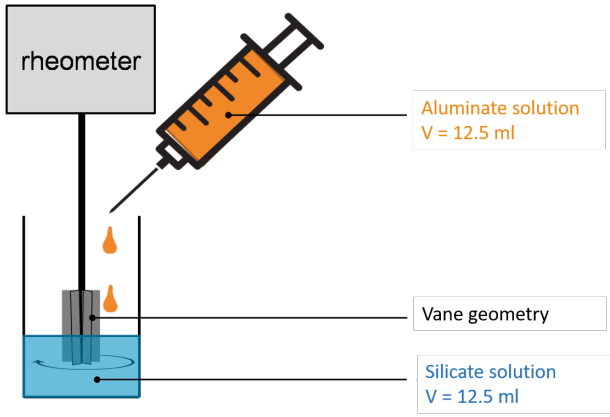

Fig. S1: Schematic representation of the *in situ* formulation in rheometer

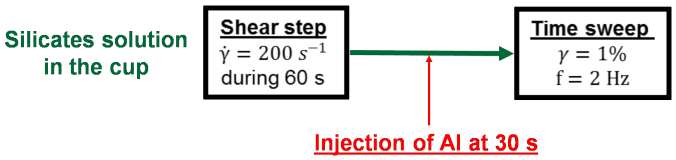

Fig. S2: Protocol for the time sweep experiments

2 Influence of the method of preparation of the gel

Figure S3 present the influence of the addition of sodium hydroxide on the kinetic of gelation, when NaOH is introduced either in the silicate solution or in the aluminate solution. As discussed in the main text, the silicate species decondensate by increasing the hydroxide content, producing more reactive and mobile species in the system. When adding the silicate solution, the gelation is then faster, with respect to the addition of an excess of sodium hydroxide in the aluminate solution. However, the mechanical properties are the same at the end of the gelation, meaning that it is the final concentration of chemical species in the gel that drives its final mechanical properties.

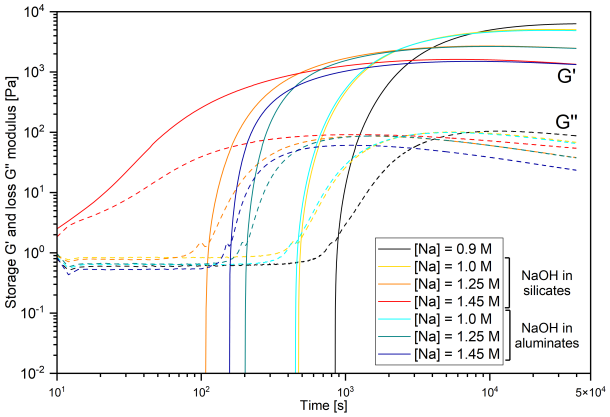

Fig. S3: Kinetic of gelation if an excess of NaOH is introduced either in the silicate solution or in the aluminate solution. [Si] = 1.125 mol·L^{-1}, [Al] = 0.12 mol·L^{-1}

3 Homogeneous vs inhomogeneoud gels

Fig. S4: Photos of homogeneous gel (solid red zone of ternaries diagrams) and inhomogeneous gel (red hatched zone of ternaries diagrams)

4 Effect of the temperature on the viscoelastic modulus

The kinetic of gelation is faster when the temperature increases, but the values of G' ang G" on the mature gel seem independent of the temperature, as reported on Figure S5 A. From these experiments and for various chemical formulations, we were able to calculate the activation energy from an Arrhenius plot (Figure S5 B). Ea seems independent of the chemical formulation and around 70 kJ·mol^{-1}.

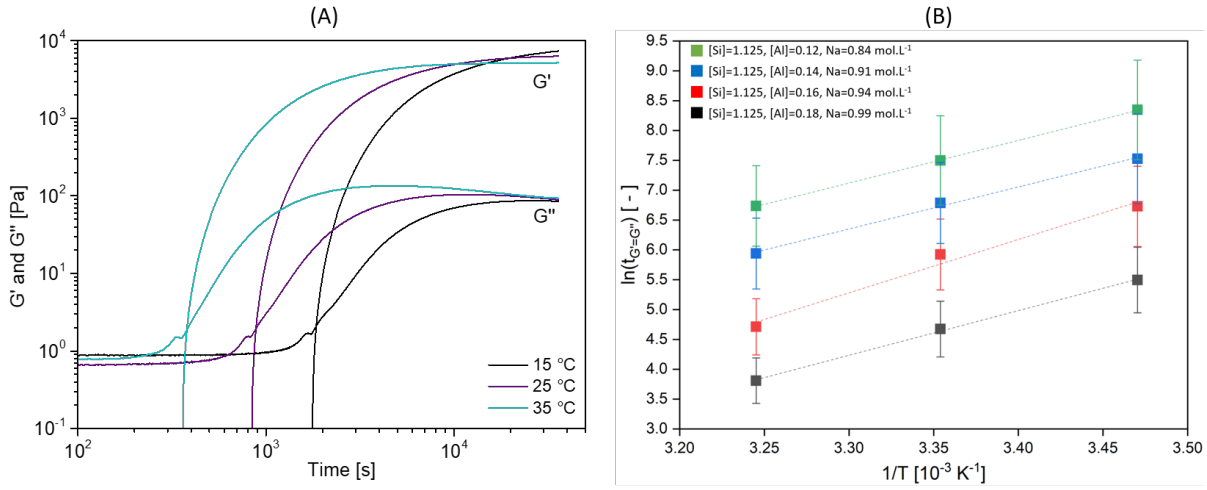

Fig. S5: (A) Temperature effect on the kinetic of gelation for the [Si] = 1.125 mol·L^{-1}, [Al] = 0.12 mol·L^{-1}, [Na] = 1.31 mol·L^{-1} formulation, (B) Activation energy for four chemical formulations

5 Fractional Gel Model (FGM) parameters

The influence of the aluminum concentration on the FGM parameters is proposed on Figure S6. $\mathbb{V}_1$=7020 Pa.s$^{\alpha}$, $\mathbb{G}_1$=643 Pa, α_1=0.39, τ_1=483 s

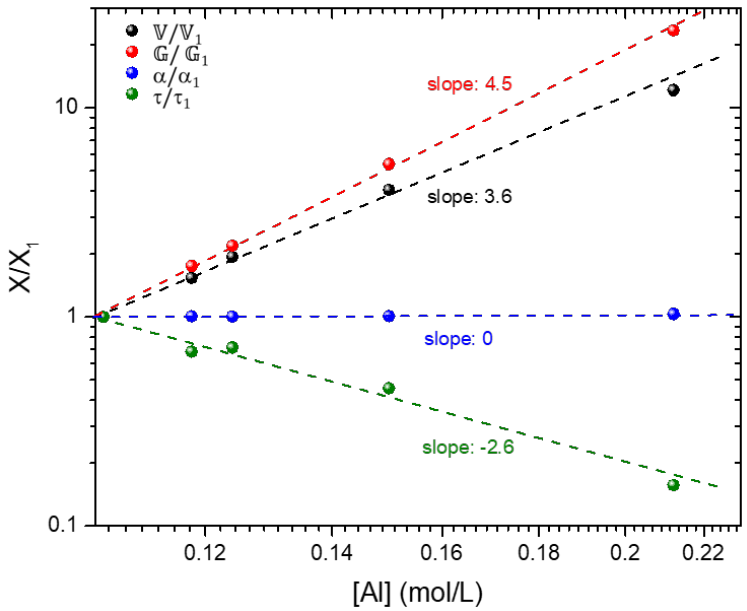

Fig. S6: τ/τ_1, α/α_1, $\mathbb{V}/\mathbb{V}_1$ and $\mathbb{G}/\mathbb{G}_1$ determined from adjustment of experimental frequency sweep with FGM model.

6 Scaling for other chemical compositions: the unbalanced set

Dimensionless master curve for five chemical formulations (unbalanced samples) is presented on Figure S7. As for the set of formulations discussed in the main text, the horizontal shift is performed by using a relaxation time calculated from the fractional gel model and the vertical shift just consists in a normalization by the elasticity at the plateau G_0.

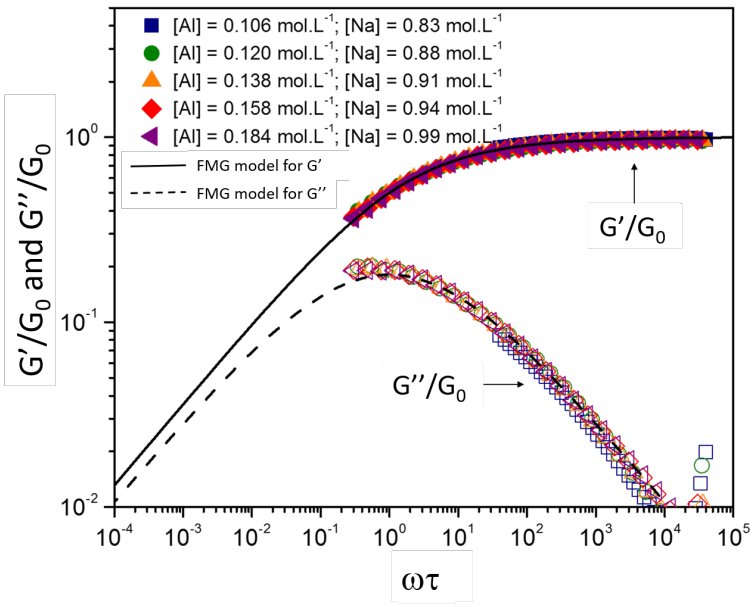

Fig. S7: Dimensionless master curve for five chemical formulations (unbalanced samples). Dimensionless values of viscoelastic moduli G'/G_0 and G''/G_0 are plotted as a function of the reduced frequency $\omega\tau$. Solid and dashed lines show the dimensionless fits of the FMG model .

7 Normalized strain sweep on the unbalanced formulations

The normalized strain sweep for the set of unbalanced formulations is presented on Figure S8. The limit of linearity decreases when the aluminum content increases, this latter roughly representing the volume fraction of particles.

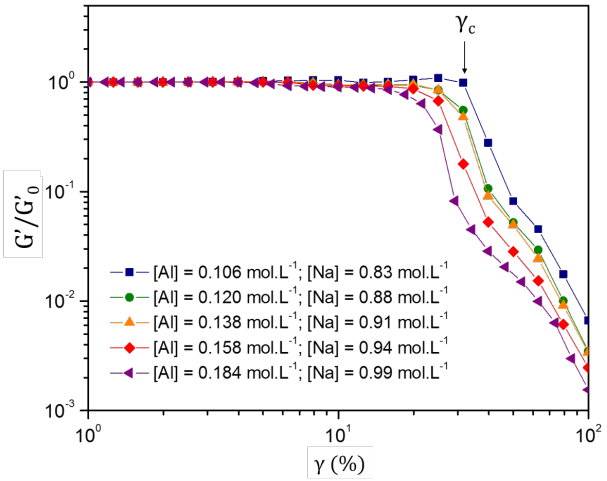

Fig. S8: Experimental G' normalized by G' at the plateau, G'/G_0, as a function of the strain γ, for various unbalanced formulations with [Si] = 1.125 mol·L^{-1}. γ_c represents the critical strain.

8 Fractional Gel Model parameters for the unbalanced formulations

For the set of unbalanced formulations, the influence of the aluminum concentration on the FGM parameters is presented in Figure S9. $\mathbb{V}_1$=54724 Pa.s^{α}, $\mathbb{G}_1$=3186 Pa, α_1=0.45, τ_1=400 s

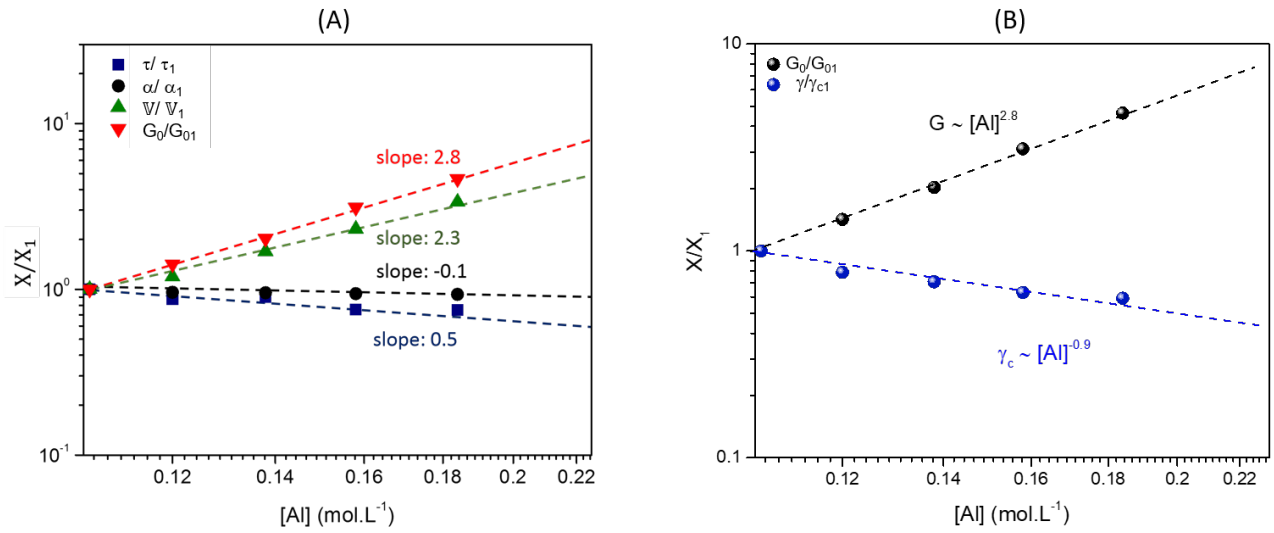

Fig. S9: τ/τ_1, α/α_1, $\mathbb{V}/\mathbb{V}_1$ and G_0/G_{01} determined from adjustments of FGM for unbalanced formulations.

In Figure S9-A we observe that the scaling exponents are lower than those for the other chemical formulations (Fig. S6). By combing the results from Figures S9-A and S8, we obtain the evolution of the elasticity and the critical strain as a function of aluminum concentration. (Fig. S9-B) with power law exponents μ=2.8 and ν=0.9. These exponents are lower than for the other set of chemical formulation suggesting a modification of the strength balance between intra and inter flocs i.e. the backbone links in the intra-clusters seem becoming stronger and their stiffness grows to a level comparable to the inter-cluster links. However, it is not completely clear yet, because both Al and Na concentrations vary concomitantly with an antagonist effect, where aluminum acts as a bond maker whereas sodium acts as a bond breaker. Indeed, the Fig. S12 shows a decrease of the viscoelastic modulus (the power law exponent is close to 5.1) as a function of the sodium concentration, even with a constant concentration of aluminum. It is thus possible that sodium ions come around the building blocks and the clusters, limiting their interaction. Nevertheless, the scattering data confirm an identical fractal dimension (d_f=2.1) for the clusters, but the cluster and building block sizes are higher for the highest concentration of sodium.

9 Influence of NaOH on the mechanical spectra and on the fractional parameters

The influence of the NaOH concentration on the frequency sweep is presented in Figure S10. Increasing the alkalinity produced a weaker gel. The fractional parameters as a function of the sodium concentration are plotted in Figure S11. Unlike the other formulations, $\mathbb{V}$ and G decrease, and the structural parameter α slightly decreases, entailing an increase of the relaxation time with higher sodium concentrations. This later result suggests that the size of the clusters is bigger, which is consistent with the USAXS data presented in the main text. $\mathbb{V}_1$=10791 Pa.s$^\alpha$, G_{01}=1128 Pa, α_1=0.39, τ_1=329 s.

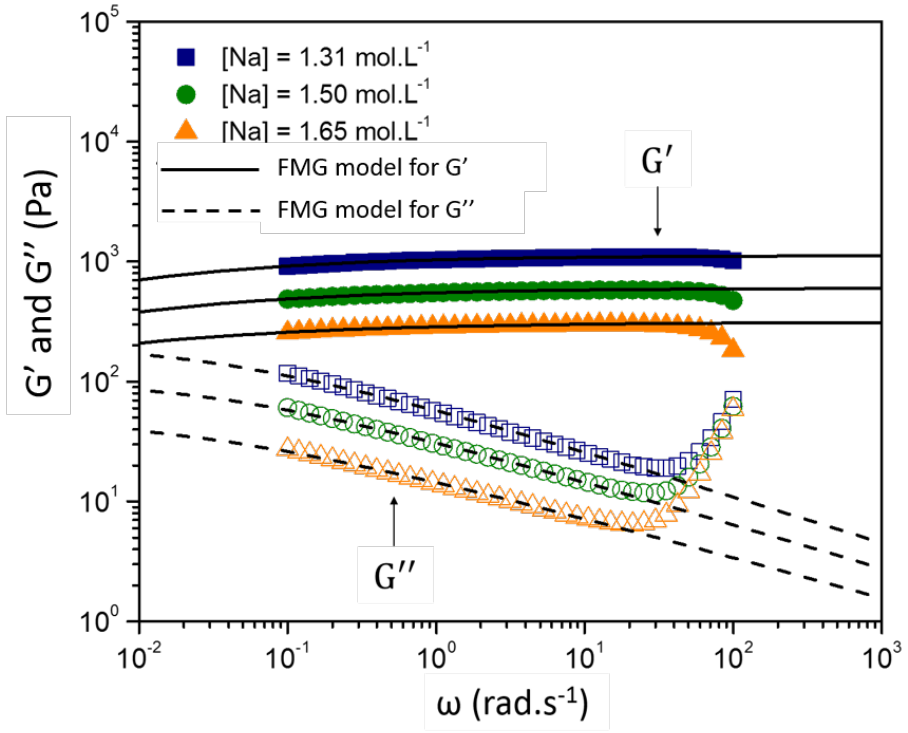

Fig. S10: Viscoelastic modulus as a function of frequency, for various sodium concentrations with [Si] = 1.125 mol·L^{-1} and [Al] = 0.118 mol·L^{-1}. Fractional Gel Models are used to describe the experimental data.

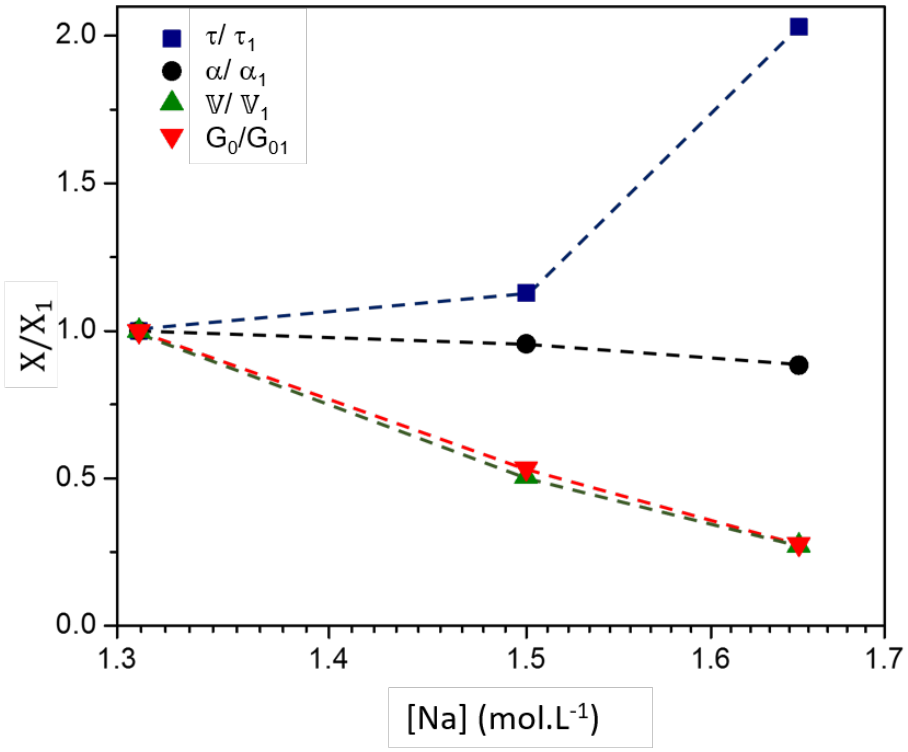

Fig. S11: Influence of sodium concentration on the FGM model parameters: τ/τ_1, α/α_1, $\mathbb{V}/\mathbb{V}_1$ and G_0/G_{01},

10 USAXS data treatment

The scattering intensity over the whole q-range (USAXS data in Figure 7) is modeled by Eq. SI-1, Keshavarz *et al.* (2021). The first term is a Porod law describing the surface scattering of a superstructure. The second term uses a Guinier-Porod model Hammouda (2010) that interpolates between a Guinier regime at low q and a power-law Porod scaling at large q.

The crossover between the two regimes is controlled by a characteristic length scale R_g. In order to account for successive structural levels covering different ranges of length scales, two structural levels in the intermediate q range were used. A structure factor $S(q)$ is also used in this model to take into account the correlation between entities inside the clusters. The third term is also a Guinier-Porod model used to describe the small silicate entities remaining in the solution that do not participate to the gel scattering.

$$I(q) = \frac{A}{q^4} + \left[\frac{G_2}{q^{s_2}} \exp\left(-\frac{q^2 R_{g,2}^2}{3-s_2}\right) + \frac{G_1}{q^{s_1}} \exp\left(-\frac{q^2 R_{g,1}^2}{3-s_1}\right) + \frac{B}{q^{d_1}}\right] S(q) + \frac{G_0}{q^{s_0}} \exp\left(-\frac{q^2 R_{g,0}^2}{3-s_0}\right) + \frac{C}{q^{d_0}} \quad (1)$$

where

$$G_2 = G_1 \exp\left[-q_2^2\left(\frac{R_{g,1}^2}{3-s_1} - \frac{R_{g,2}^2}{3-s_2}\right)\right] q_2^{(s_2-s_1)}, \quad B = G_1 \exp\left(-\frac{q_1^2 R_{g,1}^2}{3-s_1}\right) q_1^{(d_1-s_1)}, \quad C = G_0 \exp\left(-\frac{q_0^2 R_{g,0}^2}{3-s_0}\right) q_0^{(d_0-s_0)} \quad (2)$$

and

$$q_2 = (s_1-s_2)^{1/2}\left[\frac{2R_{g,2}^2}{3-s_2} - \frac{2R_{g,1}^2}{3-s_1}\right]^{-1/2}, \quad q_1 = \frac{1}{R_{g,1}}\left[\frac{(d_1-s_1)(3-s_1)}{2}\right]^{1/2}, \quad q_0 = \frac{1}{R_{g,0}}\left[\frac{(d_0-s_0)(3-s_0)}{2}\right]^{1/2} \quad (3)$$

where q_i represent the transition regions for describing each level of scattering with $q_2 \leq q_1 \leq q_0$. From the point of view of the characteristic length-scales, this means that $R_{g,2} \geq R_{g,1} \geq R_{g,0}$. A, B and C are the Porod constants and G_1, G_0 are fitting constants. The values of s_i with $i = 0, 1$ and 2 represent the structural parameters used to model non spherical objects. Values of $R_{g,i}$ with $i = 0, 1$ and 2 are the radii of gyration and d_0 and d_1 represent the Porod exponent for level 0 and 1 respectively.

An empirical structure factor was used to take into account the appearance of some correlated regions after the critical point (sol/gel transition). The expression for $S(q)$ is given by:

$$S(q) = 1 + C_0\left[\left(\frac{q}{q_0}\right)^2 + \left(\frac{q}{q_0}\right)^{-2}\right]^{-1} \quad (4)$$

where C_0 is a constant and q_0 is the position of the maximum of the correlation peak. This expression leads to the following asymptotic limits:

$$\lim_{q\to\infty} S(q) = 1, \quad \lim_{q\to 0} S(q) = 1 \quad \text{and} \quad S(q) = 1 + \frac{C_0}{2} \quad \text{for} \quad q = q_0$$

The measured USAXS data are fitted with the scattering model (1) and the fitting parameters for the chemical compositions presented in Figure 7 are tabulated in Table S1.

Table S1: Fitting parameters of the scattering model fitted to the USAXS data of various chemical compositions.

Aluminosilicate gels	A	G_1	G_0	$R_{g,2}$ (Å)	$R_{g,1}$ (Å)	$R_{g,0}$ (Å)	s_2	s_1	s_0	d_1	d_0	C_0	q_0
1. $Si_{1.125}$-$Al_{0.12}$-$Na_{1.65}$	0.0	0.02	0.17	2772	24.2	3.95	0.5	2.1	0.0	4.0	2.0	0.6	0.02
2. $Si_{1.125}$-$Al_{0.106}$-$Na_{0.83}$	0.0	0.028	0.16	685	17.7	4.3	0.2	2.0	0.0	4.0	2.0	2.0	0.04
3. $Si_{1.125}$-$Al_{0.106}$-$Na_{1.31}$	0.0	0.0155	0.15	1700	18.1	3.85	0.4	2.1	0.0	4.0	2.45	1.3	0.023

11 Influence of the chemistry on the elasticity at equilibrium

The influence of each chemical element, while keeping the two other constant, on the elastic modulus at equilibrium is presented in Figure S12. We observe a power law dependency of the elasticity of the gel, with a negative exponent for the effect of Na, and a positive exponent for both Al and Si.

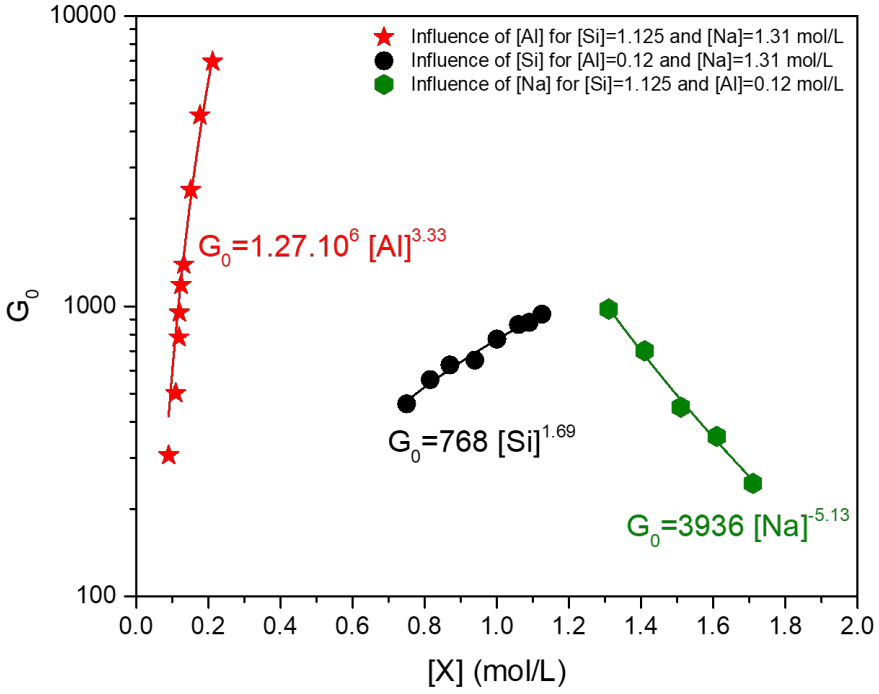

Fig. S12: Elastic modulus at equilibrium, for varying concentration of each chemical while keeping the two other constant. X correspond to either Al, Si or Na

12 Evolution of the gel volume over time

The evolution of the volume of the gel as a function of time is presented in Figure S13. The destabilization of the gel seems to be postponed when the sodium concentration if low.

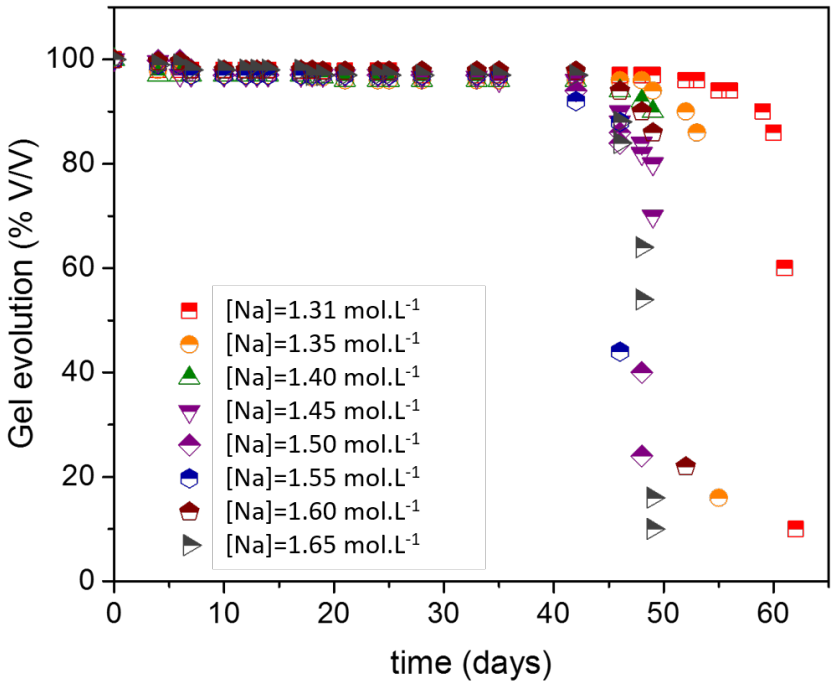

Fig. S13: Volume occupied during the early aging at 40 °C, for gels formulated with various sodium concentrations in [Si] = 1.125 mol·L^{-1} and [Al] = 0.118 mol·L^{-1}

13 X-Ray Diffraction patterns of the zeolites synthesized at 40 and 50 °C

The influence of the initial concentration of aluminum and sodium on the XRD patterns for samples synthesized at 40 and 50 °C is presented on Figures S14, S15, and S16. For the synthesis led at 40 °C, it is observed that whatever the initial concentration of aluminum and sodium, the main crystalline precipitate is Chabazite. At 50 °C, additionnal peak of Gmelinite (presenting exactly the same stoechiometry of chabazite but that do not crystallized in the same space) is observed around 2theta=27 degree. The XRD patterns do not seem modified by the increase of the aluminum concentration, whereas an increase of the initial sodium amount yields to a narrowing of the peaks centered around $2\theta \sim 9$, 21, 53° (Figures S14 and S15). The peak narrowing is related to an increase of the crystalline domain size Holder and Schaak (2019), that is also coherent with the USAXS results presented in the main text. At 50 °C, the transformation of the zeolite particles (between 20-24° in 2θ among others) into Chabazite type is noticed. The Figure S17 specifically compares the influence of the aging temperature for two concentrations of aluminum. The diffraction peaks are narrower at 40 °C meaning the size of cristallites are larger. This is certainly due to the fact that at low temperature the zeolites have more time to nucleate and growth (zeolites precipitate in 60 days at 40 °C with respect to 30 days at 50 °C).

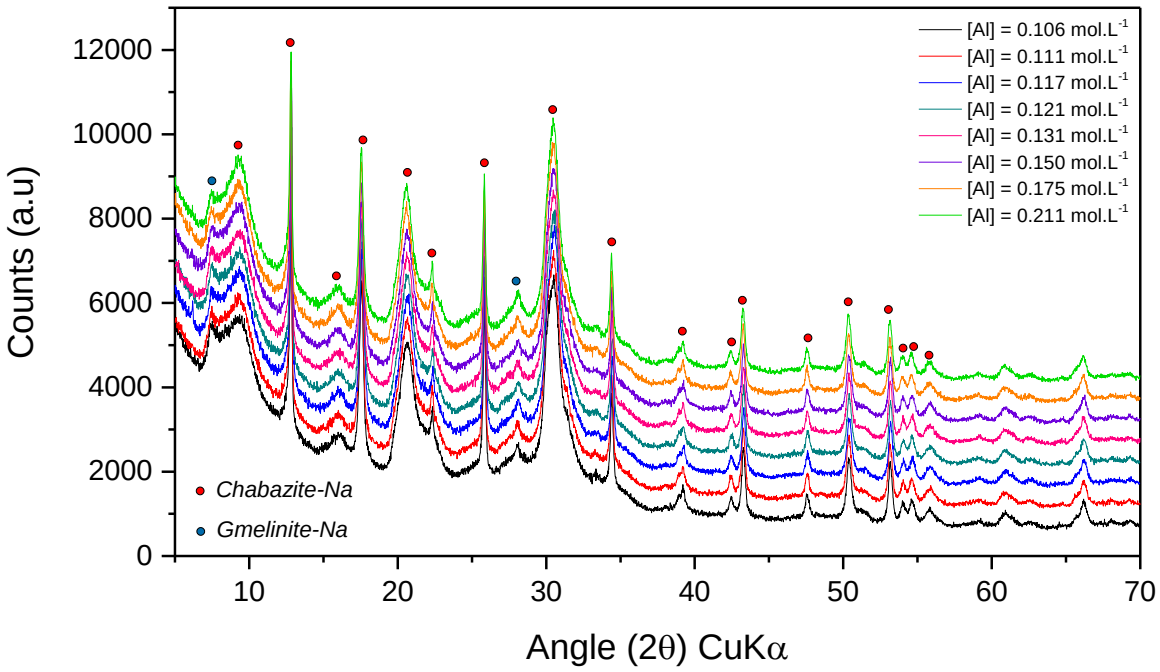

Fig. S14: Influence of aluminum concentration on the XRD patterns of aluminosilicate crytals obtained after aging at 40 °C. [Si] = 1.125 mol·L^{-1} and [Na] = 1.31 mol·L^{-1}

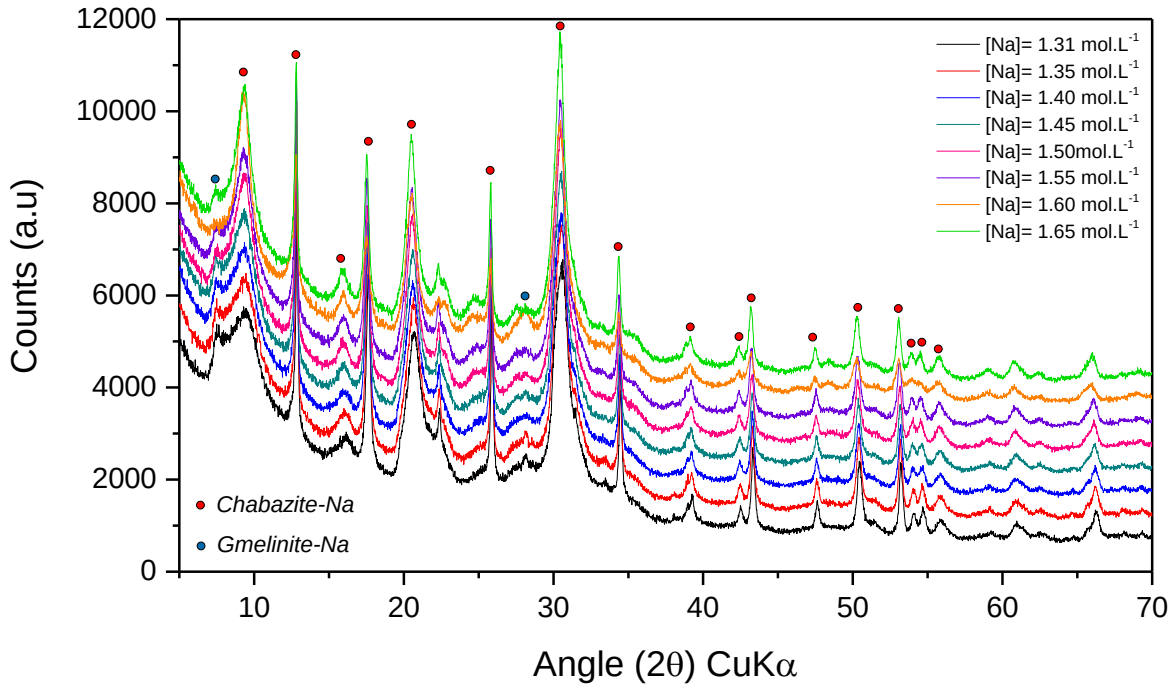

Fig. S15: Influence of sodium concentration on the XRD patterns of aluminosilicate crytals obtained after aging at 40 °C. [Si] = 1.125 mol·L^{-1} and [Al] = 0.12 mol·L^{-1}

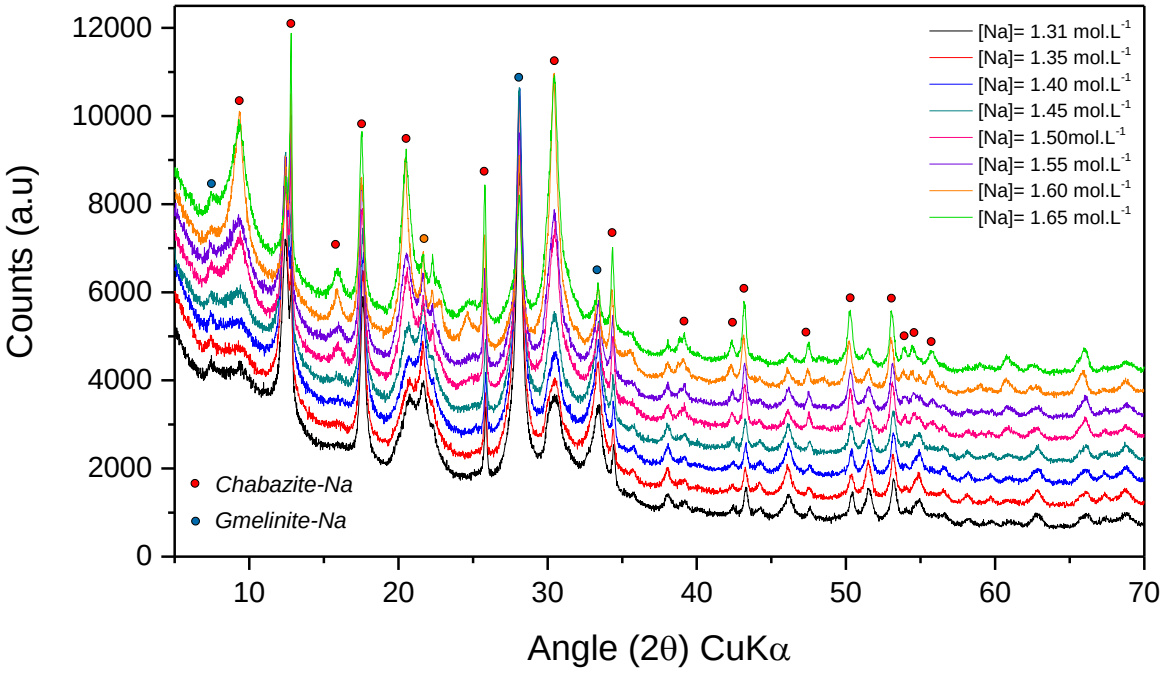

Fig. S16: Influence of sodium concentration on the XRD patterns of aluminosilicate crytals obtained after aging at 50 °C. [Si] = 1.125 mol·L^{-1} and [Al] = 0.12 mol·L^{-1}

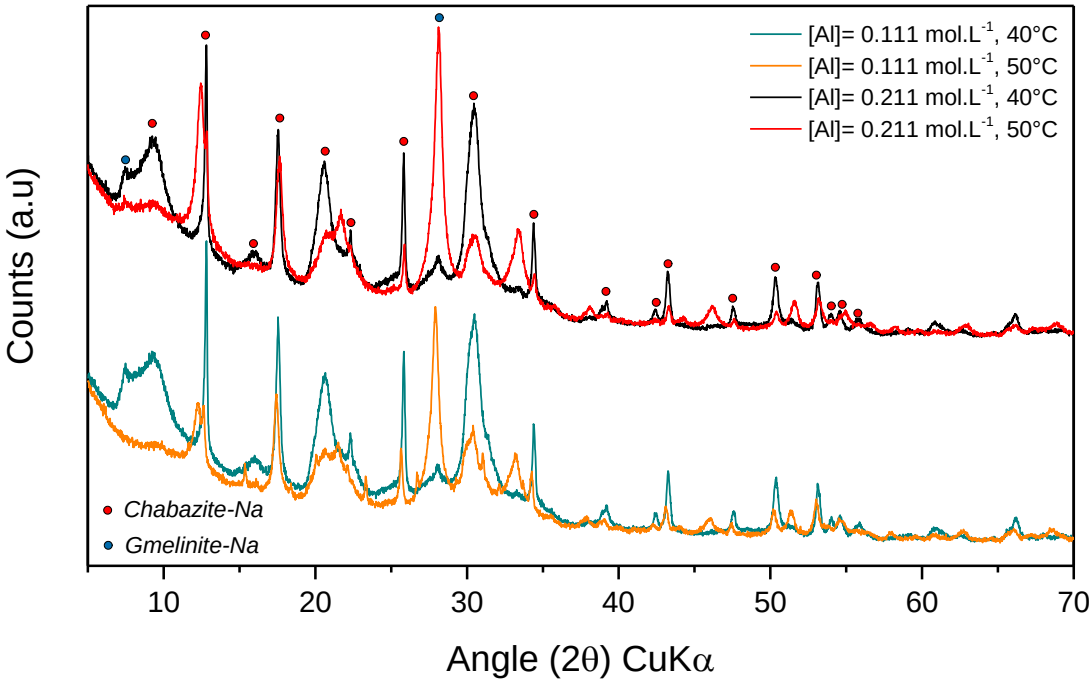

Fig. S17: Influence of the cure temperature on the diffraction patterns for two concentrations of aluminum. [Si] = 1.125 mol·L^{-1} and [Na] = 1.31 mol·L^{-1}

References

B. Keshavarz, D. G. Rodrigues, J.-B. Champenois, M. G. Frith, J. Ilavsky, M. Geri, T. Divoux, G. H. McKinley and A. Poulesquen, *Proceedings of the National Academy of Sciences*, 2021, **118**, e2022339118.

B. Hammouda, *Journal of Applied Crystallography*, 2010, **43**, 716–719.

C. F. Holder and R. E. Schaak, *ACS Nano*, 2019, **13**, 7359–7365.